Serial Magnetic Resonance Spectroscopy Reveals a Direct Metabolic Effect of Cediranib in Glioblastoma

Heisoog Kim[1,2], Ciprian Catana[2], Eva-Maria Ratai[2], Ovidiu C. Andronesi[2], Dominique L. Jennings[2], Tracy T. Batchelor[3], Rakesh K. Jain[4], and A. Gregory Sorensen[2]

Abstract

Proton magnetic resonance spectroscopy is increasingly used in clinical studies of brain tumor to provide information about tissue metabolic profiles. In this study, we evaluated changes in the levels of metabolites predominant in recurrent glioblastoma multiforme (rGBM) to characterize the response of rGBM to antiangiogenic therapy. We examined 31 rGBM patients treated with daily doses of cediranib, acquiring serial chemical shift imaging data at specific time points during the treatment regimen. We defined spectra from three regions of interest (ROI)—enhancing tumor (ET), peritumoral tissue, and normal tissue on the contralateral side (cNT)—in post-contrast T1-weighted images, and normalized the concentrations of *N*-acetylaspartate (NAA) and choline (Cho) in each ROI to the concentration of creatine in cNT (norCre). We analyzed the ratios of these normalized metabolites (i.e., NAA/Cho, NAA/norCre, and Cho/norCre) by averaging all patients and categorizing two different survival groups. Relative to pretreatment values, NAA/Cho in ET was unchanged through day 28. However, after day 28, NAA/Cho significantly increased in relation to a significant increase in NAA/norCre and a decrease in Cho/norCre; interestingly, the observed trend was reversed after day 56, consistent with the clinical course of GBM recurrence. Notably, receiver operating characteristic analysis indicated that NAA/Cho in tumor shows a high prediction to 6-month overall survival. These metabolic changes in these rGBM patients strongly suggest a direct metabolic effect of cediranib and might also reflect an antitumor response to antiangiogenic treatment during the first 2 months of treatment. Further study is needed to confirm these findings. *Cancer Res; 71(11); 3745–52. ©2011 AACR.*

Introduction

Glioblastoma multiforme (GBM) is a severe and generally fatal brain tumor, with an annual incidence of approximately 9,000 in the United States. Despite aggressive treatment strategies involving surgery, radiation, and cytotoxic chemotherapy, the average survival time for a patient with GBM is less than 1 year, and fewer than 5% of patients survive 5 years or more (1). Innovative therapeutic approaches are desperately needed for this patient population. GBM is typically characterized by marked angiogenesis and, paradoxically, severe hypoxia and necrosis (2–5). Angiogenesis in GBM is mediated by VEGF (6–8), which leads to dysfunctional and highly permeable microvessels, characterized by abnormalities in pericyte coverage and basement membrane thickness (2, 9–11).

Bevacizumab, a humanized monoclonal antibody that targets VEGF-A ligand, was approved by the FDA in May 2009 for use as a monotherapy for recurrent GBM (rGBM), on the basis of phase II evaluations (12). However, the mechanisms by which antiangiogenic therapies benefit these patients are not well understood. Jain and colleagues have shown that anti-VEGF therapies "normalize" the tumor vasculature. Their findings in both preclinical models and a clinical trial of rectal cancer have indicated that anti-VEGF therapy leads to reductions in microvessel density and mean blood vessel diameter, basement membrane thickness, tumor interstitial pressure, and vasculature permeability as well as enhanced pericyte coverage (10, 13, 14).

A phase II clinical trial of cediranib, a potent oral pan-VEGF receptor tyrosine kinase inhibitor, showed that vascular normalization was induced at 24 hours and lasted to 28 days in recurrent GBM patients, as determined by structural and functional magnetic resonance imaging (MRI) metrics (15, 16). However, these functional and structural improvements were reversed, and the tumor reverted to an abnormal state with further continuation of cediranib therapy. These findings thus suggest there may be a "normalization window" during which delivery of chemotherapeutics may be optimized.

Authors' Affiliations: [1]Massachusetts Institute of Technology, Department of Nuclear Science and Engineering–Health Science and Technology, Cambridge; [2]Athinoula A. Martinos Center for Biomedical Imaging, Massachusetts General Hospital, Department of Radiology, Charlestown; and Departments of [3]Neurology and [4]Radiation Oncology, Massachusetts General Hospital, Boston, Massachusetts

Note: Supplementary data for this article are available at Cancer Research Online (http://cancerres.aacrjournals.org/).

Corresponding Author: Heisoog Kim, Athinoula A. Martinos Center for Biomedical Imaging, Massachusetts General Hospital, 149 13th Street, Charlestown, MA 02129. Phone: 617-724-3656; Fax: 617-726-7422. E-mail: heisoog@nmr.mgh.harvard.edu

doi: 10.1158/0008-5472.CAN-10-2991

A preclinical study of GBMs in mice showed that use of cediranib can lead to a decrease in edema by vascular normalization as well as prolonged survival, even as tumor growth persists (17). The study suggested that the benefits of antiangiogenic therapies might be partially due to anti-edema effects rather than direct antitumor effects. However, other investigators have noted direct antitumor effects of VEGF blockade (18), as well as tumoristatic activities—that is, tumor growth inhibition and tumor cell apoptosis—in a broad range of human tumors (19–21), and a possible inhibitory effect on stem cell–like glioma cells (22). Thus, although the extent of vascular normalization after one dose of cediranib correlates with both progression-free survival and overall survival (OS) in rGBM patients (23), underscoring the clinical importance of vascular normalization, the degree of antitumor effect, if any, beyond vascular normalization in this class of therapies remains uncertain in humans.

Early magnetic resonance spectroscopy (MRS) studies showed clear differences between the spectral profiles of tumor and normal brain tissues. For example, choline (Cho) is typically elevated in brain tumors and metastases, potentially because of increased cellular turnover and the accelerated membrane synthesis that occur in rapidly dividing cancer cells (24, 25). Levels of *N*-acetylaspartate (NAA), regarded as a neuronal marker, decrease in any disease that adversely affects neuronal integrity (26). Hence, relative to normal healthy brain tissue, neoplastic tissue generally exhibits elevated Cho concomitant with decreased NAA (27), a hallmark widely used in clinical practice. Given these metabolic characteristics of tumors, proton MRS (^{1}H-MRS) may be able to improve demarcation of cancerous brain tissue when used in combination with the high-quality anatomic data provided by conventional MRI techniques.

In this study, we compared ^{1}H-MRS data and conventional MRI data in a group of patients undergoing cediranib monotherapy for rGBM. Our results suggest that ^{1}H-MRS confirms the findings from MRI and provides additional information to improve understanding of cancer responses to antiangiogenic agents in rGBM patients.

Materials and Methods

Patient recruitment

Thirty-one patients (mean age, 53.7; range, 20–77) with rGBM were recruited for this study. Every patient underwent surgical resection and radiochemotherapy after initial diagnosis and pathologic confirmation of GBM. At the time of enrollment into the study, all patients had tumor recurrence, as determined by MRI and/or neurologic deterioration.

All patients received an oral dose of cediranib (45 mg) daily, which was reduced as necessary (15, 16) until there was radiographic or clinical evidence of disease progression. Neurologic and physical examinations and MRI studies were done throughout the course of treatment.

MRI and spectroscopy

Magnetic resonance studies were done by using a 3T MRI scanner (Tim Trio; Siemens) at a series of time points: −5, −1, 1, 26 to 28, 54 to 56, and 110 to 112 days from the start of cediranib treatment.

We conducted serial 2-dimensional (2D) chemical shift imaging (28) by using point-resolved spectroscopy (29) for signal prelocalization and outer volume saturation (30) to minimize contamination from subcutaneous fat. Water suppression was achieved with a modified chemical selective saturation (31) method known as water suppression enhanced through T1 effects (32). Acquisition parameters included weighted k-space sampling time to repetition and time to echo in spin (TR/TE) = 1,700/135(144) ms, number of acquisition = 3, nominal resolution $1 \times 1 \times 1.4$ cm^3. First- and second-order shimming was done automatically, followed by manual adjustment. Data selected for analysis had a typical full width at half maximum in the range of 20 Hz for the water line.

The MRI protocols used conventional sequences (T1, T2, fluid-attenuated inversion recovery (FLAIR) post-Gd T1, and volumetric post-Gd image) and dynamic sequences (dynamic contrast enhanced, dynamic susceptibility contrast, and diffusion tensor imaging), as reported by Batchelor and colleagues (refs. 15, 16; see details in Supplementary Data A).

Data analysis

For 11 of 31 patients, MRS quality was inadequate to reliably detect distinct signals from the metabolites in the tumor. In some of these patients, MRS quality was compromised by tumor location near the skull; because in these cases, shimming could not be adequately carried out, the signal was considerably contaminated by fat (5 of 11 patients). In addition, in some patients, marked necrosis in the lesion caused indistinguishable peaks in the spectra (8 of 11 patients). Those spectra were objectively excluded from the data before further processing to ensure reliable analysis. The spectra obtained from 20 of the total group of 31 subjects were included in quantitative measurements.

We analyzed the spectroscopic raw data by using LC Model 6.1 Software (33), with a manual script written in Matlab. The spectra were grouped in 3 regions of interest (ROI), defined by the corresponding T1-weighted postcontrast images at baseline for (i) enhancing tumor, (ii) non-enhancing surrounding tumor (peritumoral tissue), and (iii) normal tissue on the contralateral side of tumor. The location and numbers of the voxels in each ROI were serially consistent across all time points, although there were changes in the intensity of enhancement as a consequence of treatment. To accurately assess tumor metabolism, the voxels in the enhancing tumor were selected so as to avoid areas of necrosis, hemorrhage, calcification, cysts, or ventricles. Only fitted spectra with SD (% SD) lower than 25%, per Cramér–Rao lower bounds automatically provided by the LC model, were accepted. There was no subjective spectral apodization. The concentrations of all metabolites were normalized to the normal side creatine concentration (norCre).

We examined the changes in metabolite concentrations during treatment by analyzing the ratio of NAA to Cho and the ratios of NAA and Cho to norCre. Typical spectra (Fig. 1) show that the NAA peak is higher than the Cho peak in normal tissue, whereas the ratio is reversed in tumor, that is, Cho peaks above NAA.

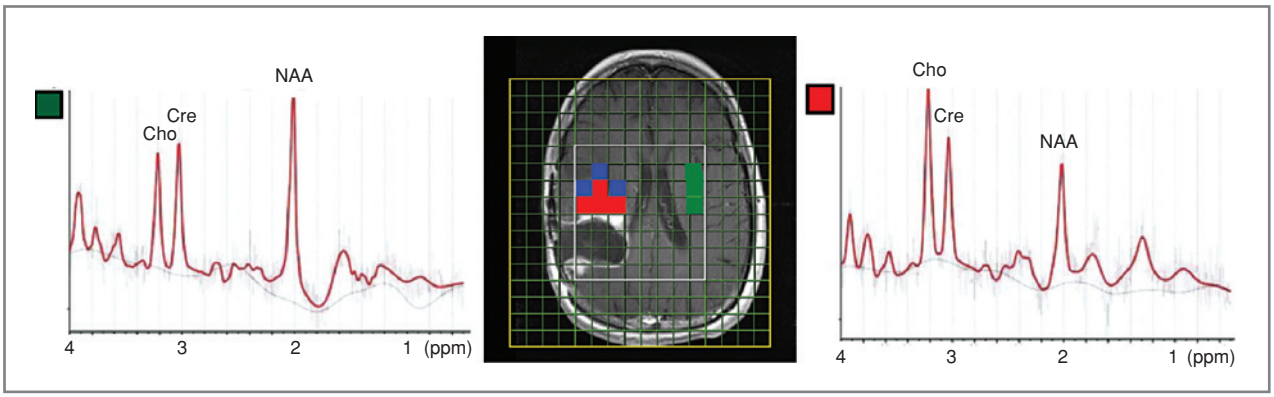

Figure 1. Three ROIs were defined on the corresponding T1-weighted postcontrast images: (i) enhancing tumor (red voxels), (ii) nonenhancing surrounding tumor-–that is, peritumoral tissue (blue voxels), and (iii) normal tissue on the contralateral side of tumor (green voxels). To obtain an accurate assessment of tumor metabolism, the voxels in enhancing tumor were selected by avoiding areas of necrosis, hemorrhage, calcification, or cysts. Typical MRS spectra were obtained from contralateral normal tissue (left) and enhancing tumor (right). These show an NAA peak higher than the Cho peak in normal tissue, whereas the ratio is reversed in the tumor; ppm, parts per million.

Changes in the MRI parameters were additionally analyzed (see details in Supplementary Data B). We assessed the vascular indexes by analyzing changes in the contrast-enhanced T1-weighted tumor (CE-T1) volume, vessel size (VS), and K^{trans} [volume transfer coefficient; in this nonflow limited state, assumed to mainly represent permeability (P)] within regions of enhancement. We quantified the water-related indexes, the functional consequences of vascular normalization, using 3 different techniques that indicate hydration level. We measured: (i) T2-weighted abnormality FLAIR, (ii) trace apparent diffusion coefficient of water (ADC), and (iii) extracellular extravascular space fraction (V_e), within regions of enhancement. We also derived the absolute T1 relaxation time constant values from variable flip angle T1 mapping sequences.

We analyzed the MRS/MRI data in relation to OS, and on the basis of the 6-month survival threshold, categorized all patients as "high OS" or "low OS" responders. Metabolite ratios on days 1, 28, and 56 were compared with baseline ratios. We computed Student t test P values against the null hypothesis, which assumes no change in metabolite ratios during treatment. The changes in MRI parameters (i.e., CE-T1, VS, P, FLAIR, ADC, and V_e) were analyzed in a similar way. Statistical significance determined by Student paired t test was accepted at a confidence level of 95% ($P < 0.05$). We conducted a receiver operating characteristic (ROC) statistical analysis to determine how predictive the MRS measurements were of 6-month survival. Numerical data were presented as average $\pm$ 1 SD. The number of subjects included in the analysis at each time point is given in Supplementary Table S1.

No corrections were made for T1 or T2, or for possible variations in water concentration between normal and tumor tissues. Our data analyses are strictly semiquantitative, as routine clinical studies do not allow for data acquisition to correct for metabolite and water relaxation. In addition, we have assumed tissue–water concentration in the tumor is similar to that in normal brain tissue; hence, we calculated only the apparent metabolite concentrations.

Results

Table 1 shows the averaged values of 3 metabolite ratios (i.e., NAA/norCre, Cho/norCre, and NAA/Cho) with SDs, the coefficients of variation, and P values tested by Student t statistics between 2 pretreatment visits in 3 ROIs. Relatively small mean differences were observed between 2 baselines, with moderate but acceptable coefficients of variation (<30%).

Figure 2 shows a representative example of serial T1 post-contrast MR images and raw spectra in 1 representative voxel (denoted by the dark-lined box) of the enhancing tumor region during the time course of treatment. The spectra display dynamic changes of peak of each metabolite in the range of 0.5 to 4 parts per million (ppm).

Figure 3 shows the changes in the NAA/norCre, Cho/norCre, and NAA/Cho ratios relative to pretreatment values, as well as lipid and lactate levels normalized by norCre, averaging across all eligible patients.

The primary metabolic index in Fig. 3A, NAA/Cho, provides a combined picture of the most commonly used diagnostic criterion of metabolic changes for some types of tumors (27, 34, 35). Many studies have reported lower NAA/Cho ratios in tumors (compared with normal tissue) because of decreased levels of NAA and/or increased levels of Cho (36–39); such findings are frequently interpreted as resulting from the replacement of normal brain tissue by cancerous tissue. Although averaged, NAA/Cho in both enhancing tumor and peritumor regions showed no significant change until 28 days; there was significant increase between days 28 and 56 ($P = 0.01$), then a subsequent decrease. In the contralateral normal tissue, NAA/Cho was relatively constant.

As illustrated in Fig. 3B, the ratio of lipids and lactate (including all lipid peaks in the range of 0.5–2 ppm) in enhancing tumor versus Cre on the contralateral normal side (norCre) decreased significantly on day 56. As in the case with other metabolites, (lipids and lactate)/norCre was relatively stable in the contralateral normal tissue.

Figure 3C and D show the individual behavior of the metabolites normalized by Cre in the contralateral tissue

Table 1. Mean and SD of NAA/norCre, Cho/norCre, and NAA/Cho for all patients in 3 ROIs

	Day −5	SD	Day −1	SD	Coefficients of variance	*P* (t-test)
NAA/norCre						
Tumor	0.77	0.33	0.77	0.23	0.27	0.66
Periphery	1.17	0.29	1.22	0.45	0.22	0.51
Normal	1.65	0.21	1.62	0.19	0.10	0.99
Cho/norCre						
Tumor	0.33	0.11	0.36	0.11	0.32	0.50
Periphery	0.33	0.09	0.35	0.11	0.25	0.57
Normal	0.35	0.06	0.35	0.08	0.08	0.38
NAA/Cho						
Tumor	2.49	0.84	2.40	0.75	0.21	0.75
Periphery	3.78	0.94	3.62	1.07	0.09	0.98
Normal	4.98	1.00	4.99	1.10	0.09	0.51

(norCre). Figure 3C illustrates a sharp increase in NAA/norCre in the enhancing tumor after a single dose of cediranib. The increase was present until day 56 ($P = 0.02$), at which time point the value began to decrease until the end of the study ($P = 0.04$). In the peritumoral region, NAA/norCre increased until day 28 and remained relatively constant close to the normal value (i.e., 1.5) until day 112 ($P = 0.04$).

In contrast, Cho/norCre (Fig. 3D) in the enhancing tumor showed a different pattern: an increase up to day 28 ($P = 0.03$), a decrease from 28 to 56 days, and then no change until the end of the study (day 112). The decrease in Cho reached statistical significance ($P = 0.047$) between days 28 and 56. A similar trend was found in the peritumoral region. In the contralateral normal tissue, both NAA/norCre and Cho/norCre remained relatively constant.

We also analyzed the changes in the MR parameters relative to baseline for the same subset of 20 patients; for reference, results are shown in Supplementary Figure S1.

The MRI data from the subset of patients from whom we also acquired analyzable MRS data were similar to the MRI findings of others in the whole 31-patient sample (16). In both the larger data set of 31 patients and the subset of 20 patients from whom we acquired MRS data, the volume of CE-T1 decreased until day 28 and thereafter began to increase. An abrupt and substantial decrease in K^{trans} (mean approximately −70%) was noted immediately after the first dose of cediranib (day 1). The relative tumor vessel size also decreased until day 28 and began to increase after day 28. We observed sustained decrease in vasogenic edema, shown by reduced FLAIR lesion volumes, ADC, and V_e for the duration of the therapy. These findings suggested a high probability of anti-permeability effects of cediranib until day 28.

We analyzed MRS/MRI findings in relation to OS times of patients on the basis of the 6-month survival threshold. Early posttreatment time points (i.e., days 1, 28, and 56) may be the most important for treatment management because early indications of therapeutic outcome provide better opportunity to optimize therapeutic intervention and improve survival (40).

As shown in Supplementary Figure S2, the MRS data indicated no significant difference in the ratios of the

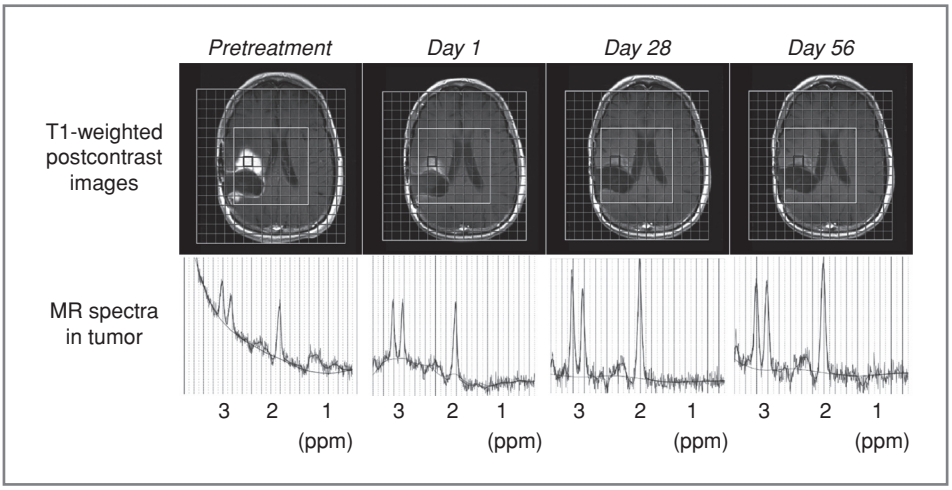

Figure 2. Serial T1 postcontrast MR images and raw spectra in one representative voxel (dark-lined box) of enhancing tumor region in the time course of treatment. The spectra exhibit the dynamic changes of peak of each metabolite in the range of 0.5 to 4 ppm at every time point of treatment.

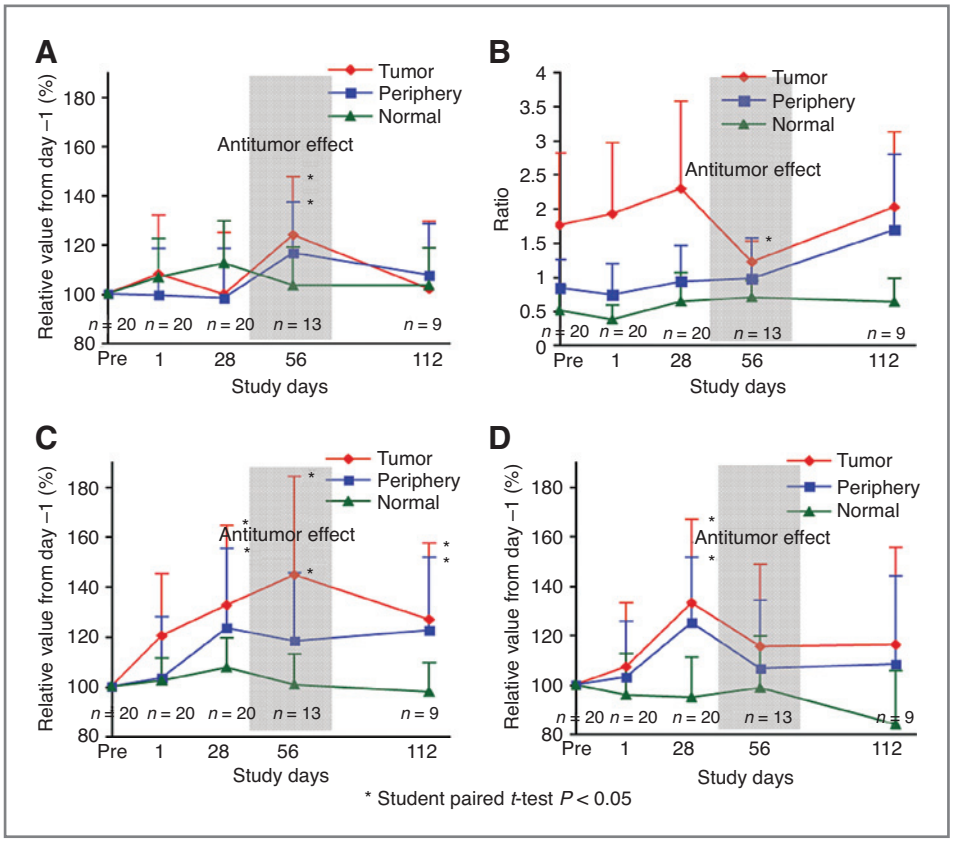

Figure 3. Averaged MRS changes over all eligible patients relative to pretreatment values (%). A, NAA/Cho; B, (lipids and lactate)/norCre; C, NAA/norCre; D, Cho/norCre. The number of the eligible patients at each time point is provided under each data point. Numerical data are presented as average ± 1 SD. *, $P < 0.05$ with Student paired *t* test.

metabolites, including NAA/norCre, Cho/norCre, and NAA in tumor/NAA in the contralateral normal tissue (tumNAA/norNAA), and Cho in tumor/Cho in the contralateral normal tissue (tumCho/norCho); similarly, the group differences in MRI measurements of "high OS" and "low OS" responders were considered as having no significant effect (Supplementary Fig. S3). However, NAA/Cho (Fig. 4), the most commonly used clinical MRS measure for discriminating normal and abnormal tissues (27), notably showed an increase in the "high OS" group (15%, 9%, and 40% with $P < 0.05$ on days 1, 28, and 56, respectively), although showing a decrease in the "low OS" group (−12%, −10%, and −20% on days 1, 28, and 56, respectively). On the basis of this finding, we carried out ROC analysis to determine the probability that NAA/Cho predicts 6-month survival. In Table 2, the values of an area under the ROC curve (AUC) and *P* values at early time points, particularly days 28 and 56, showed the high possibilities (74% and 95%) and the significances (0.02 and 0.01).

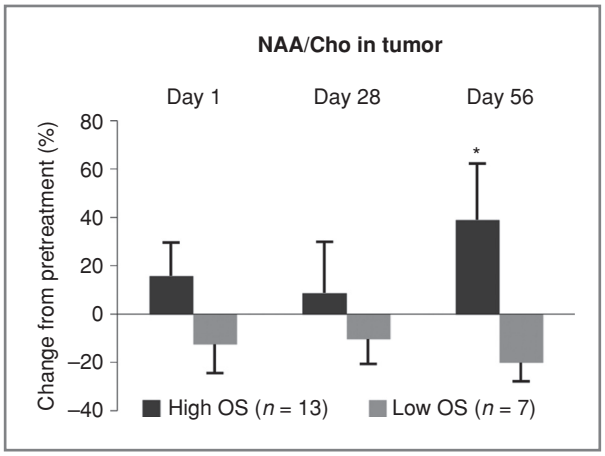

Figure 4. The relative changes (%) in NAA/Cho separately grouped by the OS periods of patients on the basis of 6-month survival threshold at the early time points posttreatment (i.e., days 1, 28, and 56) in the enhancing tumor region.*, $P < 0.05$ with Student paired *t* test.

We compared the relative changes in the ratios of the 3 metabolites before and after 1 dose of cediranib to the changes in the absolute values of norCre and the T1 relaxation time constant in Supplementary Figure S4. The comparison showed subtle changes in norCre and T1 time constant after one dose, confirming that changes in NAA/norCre are independent of norCre and T1 changes.

Discussion

In this clinical study, we sought to identify metabolic changes in rGBM, using MRS to distinguish the changes induced by cediranib treatment. We observed elevated Cho, lactate, and lipid peaks, with very low NAA peak, in enhancing lesions and a reverse metabolite profile in contralateral normal tissue at baseline. The mean values of NAA/Cho were 2.4 in the enhancing tumor and 5.0 in normal tissue. These results mirror

Table 2. AUC on early time points determine the prediction of NAA/Cho to 6-month survival

NAA/Cho	1 day	28 days	56 days
AUC	0.68	0.74	0.95
(95% CI)	(0.65–0.72)	(0.71–0.78)	(0.91–1.00)
P	0.15	0.02	0.01

the classic patterns of metabolite peaks seen in high-grade gliomas and the mean values that have been measured in other published reports (27, 39, 41–43). Our results also confirm the ability of MRS to evaluate tumor response to treatment (27, 39, 44–48). Our results both extend earlier studies to track metabolic changes induced by an antiangiogenic agent in tumor tissue and report several new findings.

The first new observation is the consistency of the NAA/Cho ratio with increased concentration of both Cho and NAA in tumoral as well as peritumoral regions during the vascular normalization window of 28 days (15). One interpretation of these findings is that tumor cells are not directly killed during the initial normalization window, and the marked changes in tumor enhancement observed in conventional MRI reflect antivascular effects of the antiangiogenic drug. This interpretation is compatible with preclinical results reported (17). The decrease in tumor size and the consequential shift in brain seen until 1 month after treatment initiation might reasonably prompt one to conclude that NAA/norCre and Cho/norCre increases are attributable to partial volume effects. A statistically significant decrease in hydration level (i.e., vasogenic edema, as seen by ADC) during 1 month may also account for these changes.

The second observation is a significant increase in NAA/Cho, with a significant reduction in Cho and an increase in NAA after 28 days. This finding suggests that cediranib has a direct effect on cellular metabolism in rGBM patients—an effect that is temporally separated from its anti-vascular effects and distinct from preclinical models of cediranib—possibly because of the longer survival times seen in humans compared with animal models of GBM. Further evidence of this direct metabolic effect is supported by a significant decrease in observed lipids and lactate after day 28; it has been previously shown that the spectra from active GBM contain elevated peaks of lipids (27, 42). Snuderal and colleagues (submitted manuscript) observed reduced cellular density in the central area of the tumor in the autopsies of 5 cediranib-treated patients included in our study population. This morphologic finding is consistent with the metabolic changes we detected. Also of note is that the delayed antitumor effect associated with antiangiogenic treatment has also been reported in other tumor types (49, 50).

Interestingly, ADC in MRI showed a decrease, primarily because of the significant antipermeability effect of cediranib, overwhelming its cytotoxic effect, as an increase in ADC has been shown to correlate with cell-killing mechanism for cytotoxic therapies. At baseline, the value of ADC was already high and after edema greatly reduced, ADC dropped to a normal level especially within 28 days, indicating a window of vascular normalization. However, between 28 and 56 days, there was no significant decrease in ADC; in fact, we observed a slight increase in the responding group, which was likely related to the cytotoxic mechanism of cediranib. Therefore, considering the different mechanisms of antiangiogenic and cytotoxic therapies, there would not be a complete discrepancy between ADC and ^{1}H-MRS.

The trend we observed in the MRS data was reversed after day 56, consistent with the general clinical course of tumor recurrence and the eventual death of the patients. These findings might imply that, although cediranib does have direct effects on metabolism in some tumor cells, those cells that survive despite blocked angiogenesis are eventually able to continue to grow.

A third observation in our study is the high probability of NAA/Cho to predict 6-month survival of rGBM patients treated by cediranib, as determined by ROC analysis. The changes in NAA/Cho illustrated in Fig. 4 showed positive values in "high OS" responders compared with negative values in the "low OS" group. A ROC analysis of NAA/Cho showed high significances on day 28 ($P = 0.02$, AUC = 0.74) and day 56 ($P = 0.01$, AUC = 0.95). Together, these data might imply that it is the critical time frame between 28 and 56 days that discriminates the tumor response to this antiangiogenic agent. This finding suggests that NAA/Cho has good correlation with tumor responses for predicting 6-month survival on the antiangiogenic treatment, reflecting a combined picture for the opposite changes of 2 primary metabolites.

We acknowledge that this study is limited by its small sample size and, more importantly, by our still-incomplete understanding of the correlations between MRS findings and tissue morphology. The conventional interpretations of the MRS findings in glioblastoma were generated primarily in the pre-antiangiogenic era. Although a direct antitumor effect is the interpretation most consistent with our MRS findings in this study, we cannot at this stage rule out other possible interpretations and additional studies with larger sample sizes are warranted.

This prospective study provides preliminary evidence that cediranib elicits direct metabolic effects in rGBM; traditionally such findings have been interpreted as antitumor effects resulting from vascular normalization based on the dynamics of the predominant brain metabolites. Our data also suggest that, with further technical advances, early changes in metabolites detectable by ^{1}H-MRS might be able to serve as imaging biomarkers to predict treatment response in patients with recurrent malignant GBMs. NAA/Cho changes in enhancing tumor tissues suggest that anti-VEGF therapy not only has an antivascular effect but also that such an effect modulates tumor and brain tissue, both early and late in the disease process. These findings, if confirmed in larger studies, could shed further light on the mechanism of action of this new class of antiangiogenic agents and potentially even be used to make treatment management decisions.

Disclosure of Potential Conflicts of Interest

No potential conflicts of interest were disclosed.

Acknowledgments

We thank Wei-ting Zhang and Meiyun Wang for sharing their MRI data and analysis. We specially thank Nichole Eusemann for her excellent help with revising our manuscript.

Grant Support

The work was financially supported by NIH grants R21 and K24, and by the Harvard Catalyst grant.

The costs of publication of this article were defrayed in part by the payment of page charges. This article must therefore be hereby marked *advertisement* in accordance with 18 U.S.C. Section 1734 solely to indicate this fact.

Received August 13, 2010; revised February 11, 2011; accepted March 27, 2011; published OnlineFirst April 20, 2011.

References

1. CBTRUS. Primary brain tumors in the United States Statistical Report [cited 2011 May 5]. Available from: http://www.cbtrus.org/reports/reports.html.
2. Plate KH, Mennel HD. Vascular morphology and angiogenesis in glial tumors. Exp Toxicol Pathol 1995;47:89–94.
3. Rampling R, Cruickshank G, Lewis AD, Fitzsimmons SA, Workman P. Direct measurement of pO2 distribution and bioreductive enzymes in human malignant brain tumors. Int J Radiat Oncol Biol Phys 1994; 29:427–31.
4. Valk PE, Mathis CA, Prados MD, Gilbert JC, Budinger TF. Hypoxia in human gliomas: demonstration by PET with fluorine-18-fluoromisonidazole. J Nucl Med 1992;33:2133–7.
5. Jain RK, di Tomaso E, Duda DG, Loeffler JS, Sorensen AG, Batchelor TT. Angiogenesis in brain tumours. Nat Rev Neurosci 2007;8:610–22.
6. Holash J, Maisonpierre PC, Compton D, Boland P, Alexander CR, Zagzag D, et al. Vessel cooption, regression, and growth in tumors mediated by angiopoietins and VEGF. Science 1999;284:1994–8.
7. Millauer B, Shawver LK, Plate KH, Risau W, Ullrich A. Glioblastoma growth inhibited *in-vivo* by a dominant-negative FLK-1 mutant. Nature 1994;367:576–9.
8. Shweiki D, Itin A, Soffer D, Keshet E. Vascular endothelial growth factor induced by hypoxia may mediate hypoxia-initiated angiogenesis. Nature 1992;359:843–5.
9. Jain RK, Booth MF. What brings pericytes to tumor vessels? J Clin Invest 2003;112:1134–6.
10. Winkler F, Kozin SV, Tong RT, Chae SS, Booth MF, Garkavtsev I, et al. Kinetics of vascular normalization by VEGFR2 blockade governs brain tumor response to radiation: Role of oxygenation, angiopoietin-1, and matrix metal loproteinases. Cancer Cell 2004;6:553–63.
11. Zagzag D, Hooper A, Friedlander DR, Chan W, Holash J, Wiegand SJ, et al. *In situ* expression of angiopoietins in astrocytomas identifies angiopoietin-2 as an early marker of tumor angiogenesis. Exp Neurol 1999;159:391–400.
12. Cohen MH, Shen YL, Keegan P, Pazdur R. FDA drug approval summary: bevacizumab (Avastin) as treatment of recurrent glioblastoma multiforme. Oncologist 2009;14:1131–8.
13. Willett CG, Boucher Y, di Tomaso E, Duda DG, Munn LL, Tong RT, et al. Direct evidence that the VEGF-specific antibody bevacizumab has antivascular effects in human rectal cancer. Nat Med 2004;10:145–7.
14. Willett CG, Duda DG, di Tomaso E, Boucher Y, Ancukiewicz M, Sahani DV, et al. Efficacy, safety, and biomarkers of neoadjuvant bevacizumab, radiation therapy, and fluorouracil in rectal cancer: a multidisciplinary phase II study. J Clin Oncol 2009;27:3020–6.
15. Batchelor TT, Sorensen AG, di Tomaso E, Zhang WT, Duda DG, Cohen KS, et al. AZD2171, a pan-VEGF receptor tyrosine kinase inhibitor, normalizes tumor vasculature and alleviates edema in glioblastoma patients. Cancer Cell 2007;11:83–95.
16. Batchelor TT, Duda DG, di Tomaso E, Ancukiewicz M, Plotkin SR, Gerstner E, et al. Phase II study of cediranib, an oral pan-VEGF receptor tyrosine kinase inhibitor, in patients with recurrent glioblastoma. J Clin Oncol 2010;28:2817–23.
17. Kamoun WS, Ley CD, Farrar CT, Duyverman AM, Lahdenranta J, Lacorre DA, et al. Edema control by cediranib, a vascular endothelial growth factor receptor-targeted kinase inhibitor, prolongs survival despite persistent brain tumor growth in mice. J Clin Oncol 2009;27:2542–52.
18. Genentech. 2009 [Slide 73 cited 2011 May 5]. Available from: http://www.fda.gov/AdvisoryCommittees/default.htm.
19. Mesiano S, Ferrara N, Jaffe RB. Role of vascular endothelial growth factor in ovarian cancer: inhibition of ascites formation by immunoneutralization. Am J Pathol 1998;153:1249–56.
20. Warren RS, Yuan H, Matli MR, Gillett NA, Ferrara N. Regulation by vascular endothelial growth factor of human colon cancer tumorigenesis in a mouse model of experimental liver metastasis. J Clin Invest 1995;95:1789–97.
21. Rowe DH, Huang J, Kayton ML, Thompson R, Troxel A, O'Toole KM, et al. Anti-VEGF antibody suppresses primary tumor growth and metastasis in an experimental model of Wilms' tumor. J Pediatr Surg 2000;35:30–2; discussion 2–3.
22. Bao S, Wu Q, Sathornsumetee S, Hao Y, Li Z, Hjelmeland AB, et al. Stem cell-like glioma cells promote tumor angiogenesis through vascular endothelial growth factor. Cancer Res 2006;66: 7843–8.
23. Gerstner ER, Duda DG, di Tomaso E, Ryg PA, Loeffler JS, Sorensen AG, et al. VEGF inhibitors in the treatment of cerebral edema in patients with brain cancer. Nat Rev Clin Oncol 2009;6:229–36.
24. Glunde K, Ackerstaff E, Mori N, Jacobs MA, Bhujwalla ZM. Choline phospholipid metabolism in cancer: consequences for molecular pharmaceutical interventions. Mol Pharm 2006;3:496–506.
25. Oh J, Henry RG, Pirzkall A, Lu Y, Li X, Catalaa I, et al. Survival analysis in patients with glioblastoma multiforme: predictive value of choline-to-N-acetylaspartate index, apparent diffusion coefficient, and relative cerebral blood volume. J Magn Reson Imaging 2004;19:546–54.
26. Howe FA, Opstad KS. 1H MR spectroscopy of brain tumours and masses. NMR Biomed 2003;16:123–31.
27. Nelson SJ. Multivoxel magnetic resonance spectroscopy of brain tumors. Mol Cancer Ther 2003;2:497–507.
28. Brown TR, Kincaid BM, Ugurbil K. NMR chemical shift imaging in three dimensions. Proc Natl Acad Sci U S A 1982;79:3523–6.
29. Bottomley PA. Spatial localization in NMR-spectroscopy *in vivo*. Ann N Y Acad Sci 1987;508:333–48.
30. Duyn JH, Gillen J, Sobering G, Vanzijl PCM, Moonen CTW. Multisection proton MR spectroscopic imaging of the brain. Radiology 1993;188:277–82.
31. Haase A, Frahm J, Hanicke W, Matthaei D. H-1-NMR chemical-shift selective (CHESS) imaging. Phys Med Biol 1985;30:341–4.
32. Ogg RJ, Kingsley PB, Taylor JS. WET, a T-1-insensitive and B-1-insensitive water-suppression method for *in vivo* localized H-1-NMR spectroscopy. J Magn Reson B 1994;104:1–10.
33. Provencher SW. Estimation of metabolite concentrations from localized *in vivo* proton NMR spectra. Magn Reson Med 1993;30: 672–9.
34. Sutton LN, Wehrli SL, Gennarelli L, Wang Z, Zimmerman R, Bonner K, et al. High-resolution 1H-magnetic resonance spectroscopy of pediatric posterior fossa tumors *in vitro*. J Neurosurg 1994;81:443–8.
35. Sutton LN, Wang Z, Gusnard D, Lange B, Perilongo G, Bogdan AR, et al. Proton magnetic resonance spectroscopy of pediatric brain tumors. Neurosurgery 1992;31:195–202.

36. Kugel H, Heindel W, Ernestus RI, Bunke J, du Mesnil R, Friedmann G. Human brain tumors: spectral patterns detected with localized H-1 MR spectroscopy. Radiology 1992;183:701–9.
37. Ott D, Hennig J, Ernst T. Human brain tumors: assessment with *in vivo* proton MR spectroscopy. Radiology 1993;186:745–52.
38. Houkin K, Kamada K, Sawamura Y, Iwasaki Y, Abe H, Kashiwaba T. Proton magnetic resonance spectroscopy (1H-MRS) for the evaluation of treatment of brain tumours. Neuroradiology 1995;37: 99–103.
39. Negendank WG, Sauter R, Brown TR, Evelhoch JL, Falini A, Gotsis ED, et al. Proton magnetic resonance spectroscopy in patients with glial tumors: a multicenter study. J Neurosurg 1996;84:449–58.
40. Chenevert TL, Stegman LD, Taylor JM, Robertson PL, Greenberg HS, Rehemtulla A, et al. Diffusion magnetic resonance imaging: an early surrogate marker of therapeutic efficacy in brain tumors. J Natl Cancer Inst 2000;92:2029–36.
41. Meyerand ME, Pipas JM, Mamourian A, Tosteson TD, Dunn JF. Classification of biopsy-confirmed brain tumors using single-voxel MR spectroscopy. AJNR Am J Neuroradiol 1999;20:117–23.
42. Tate AR, Underwood J, Acosta DM, Julià-Sapé M, Majós C, Moreno-Torres A, et al. Development of a decision support system for diagnosis and grading of brain tumours using *in vivo* magnetic resonance single voxel spectra. NMR Biomed 2006;19:411–34.
43. Castillo M, Kwock L. Proton MR spectroscopy of common brain tumors. Neuroimaging Clin N Am 1998;8:733–52.
44. Walecki J, Sokól M, Pieniazek P, Maciejewski B, Tarnawski R, Krupska T, et al. Role of short TE 1H-MR spectroscopy in monitoring of post-operation irradiated patients. Eur J Radiol 1999;30:154–61.
45. Rabinov JD, Lee PL, Barker FG, Louis DN, Harsh GR, Cosgrove GR, et al. *In vivo* 3-T MR spectroscopy in the distinction of recurrent glioma versus radiation effects: initial experience. Radiology 2002;225: 871–9.
46. Chan YL, Yeung DK, Leung SF, Cao G. Proton magnetic resonance spectroscopy of late delayed radiation-induced injury of the brain. J Magn Reson Imaging 1999;10:130–7.
47. Sijens PE, Vecht CJ, Levendag PC, van Dijk P, Oudkerk M. Hydrogen magnetic resonance spectroscopy follow-up after radiation therapy of human brain cancer. Unexpected inverse correlation between the changes in tumor choline level and post-gadolinium magnetic resonance imaging contrast. Invest Radiol 1995;30:738–44.
48. Usenius T, Usenius JP, Tenhunen M, Vainio P, Johansson R, Soimakallio S, et al. Radiation-induced changes in human brain metabolites as studied by 1H nuclear magnetic resonance spectroscopy *in vivo*. Int J Radiat Oncol Biol Phys 1995;33:719–24.
49. Kaban LB, Mulliken JB, Ezekowitz RA, Ebb D, Smith PS, Folkman J. Antiangiogenic therapy of a recurrent giant cell tumor of the mandible with interferon alfa-2a. Pediatrics 1999;103:1145–9.
50. Marler JJ, Rubin JB, Trede NS, Connors S, Grier H, Upton J, et al. Successful antiangiogenic therapy of giant cell angioblastoma with interferon alfa 2b: report of 2 cases. Pediatrics 2002;109:E37.